coatings

MDPI

Article

Surface Chemistry, Crystal Structure, Size and Topography Role in the Albumin Adsorption Process on TiO_2 Anatase Crystallographic Faces and Its 3D-Nanocrystal: A Molecular Dynamics Study †

Giuseppina Raffaini [1,2]

[1] Department of Chemistry, Materials, and Chemical Engineering "Giulio Natta", Politecnico di Milano, Piazza L. Da Vinci 32, 20131 Milano, Italy; giuseppina.raffaini@polimi.it
[2] INSTM, National Consortium of Materials Science and Technology, Local Unit Politecnico di Milano, 20131 Milano, Italy

† Dedicated to the memory of my father Mario Tancredi Raffaini.

Abstract: TiO_2 is widely used in biomaterial implants. The topography, chemical and structural properties of titania surfaces are an important aspect to study. The size of TiO_2 nanoparticles synthetized by sol–gel method can influence the responses in the biological environment, and by using appropriate heat treatments different contents of different polymorphs can be formed. Protein adsorption is a crucial step for the biological responses, involving, in particular, albumin, the most abundant blood protein. In this theoretical work, using molecular mechanics and molecular dynamics methods, the adsorption process of an albumin subdomain is reported both onto specific different crystallographic faces of TiO_2 anatase and also on its ideal three-dimensional nanosized crystal, using the simulation protocol proposed in my previous theoretical studies about the adsorption process on hydrophobic ordered graphene-like or hydrophilic amorphous polymeric surfaces. The different surface chemistry of anatase crystalline faces and the nanocrystal topography influence the adsorption process, in particular the interaction strength and protein fragment conformation, then its biological activity. This theoretical study can be a useful tool to better understand how the surface chemistry, crystal structure, size and topography play a key role in protein adsorption process onto anatase surface so widely used as biomaterial.

Keywords: protein adsorption; albumin; titania; anatase; nanocrystal; competitive adsorption; molecular dynamics simulations; biomaterials

Citation: Raffaini, G. Surface Chemistry, Crystal Structure, Size and Topography Role in the Albumin Adsorption Process on TiO_2 Anatase Crystallographic Faces and Its 3D-Nanocrystal: A Molecular Dynamics Study †. *Coatings* **2021**, *11*, 420. https://doi.org/10.3390/coatings11040420

Academic Editors: Michelina Catauro and Chang-Hwan Choi

Received: 15 March 2021
Accepted: 1 April 2021
Published: 4 April 2021

1. Introduction

Biomaterials are defined as materials intended to interface with biological systems to evaluate, treat, augment or replace any tissue, organ or function of the body [1–4]. The cells–biomaterials interactions are mediated by non-covalent protein-biomaterials interactions, a very fundamental aspect that should be taken into account in order to better understand the biocompatibility property and, eventually, the success of an implant in a human body [5–9]. In many different fields of nanomedicine, nanobiotechnology, biomaterial science [10–12], protein–biomaterials interactions are a central aspect in a broad range of applications such as drug delivery [13], tissue engineering [14–17], proteomics [18,19]. Biomaterials are composed by several different materials such as ceramics, polymers, metals and metal oxides, and of their combinations in interesting new biocompatible composite materials [20–24].

Metals and their alloys are often used as biomaterials due to their good mechanical stability, catalytic properties and biocompatibility [25–29]. It is well known that the size, crystal structure and surface properties of titanium-based biomaterials affect the biological

response. The titania surfaces can be amorphous or crystalline, and crystalline TiO_2 often comprises mixed-crystalline phases with different content of its polymorphs, in particular anatase and rutile phases, but also brookite [30–33]. In various biomedical applications, the anatase or rutile crystal phases are preferred over amorphous TiO_2 [34]. The temperature is an important factor both for the protein adhesion process on the solid surface and for the specific heat treatment to obtain the desired biomedical polymorph. Sit et al. were the first to show that there are differences in the temperature-dependent structural changes of proteins adsorbed on TiO_2 nanoparticles surfaces [35]. These changes depend on the initial interaction with the nanoparticles' surfaces, indicating then that it is important, also at theoretical level, to study both the initial interaction stage of the adsorption process and the final conformation assumed by protein adsorbed on biomaterial surfaces at longer periods. The heat treatment of the materials is also an important step for the production of biomaterials in a specific composition. The different TiO_2 polymorphs can form nanoparticles or nanocrystals [36–38]. Titanium oxide is also very interesting in biomedical applications as flat coating for biomedical devices. Heat treatment in a conventional furnace is a commonly applied method of the crystallization of titania nanosurfaces but it is time-consuming. Using the sol–gel dip-coating method Bakri et al. [39] showed that the TiO_2 films obtained crystallize in an anatase crystal structure and transform to a rutile phase at 900 °C. Recently, Catauro et al. [40,41] synthetized TiO_2 nanoparticles demonstrating that the sol–gel method is an ideal technique to prepare titania nanoparticles at low temperature, characterizing the presence of different chemical structures of coating and how it is possible to increase the particle size due to aggregation at higher temperature. Then, thanks to heat treatment using the sol–gel method, it is possible to synthetize TiO_2 nanoparticles at different content of two more common crystalline phases. Possible different interactions with a biological environment can take place and they must be studied more thoroughly, changing the composition and the size of the surface exposed to biological environment. In fact, the large surface area of nanoparticles with small size (<100 nm) enhances the cellular adhesion promoting the interaction between nanoparticles and tissues or cells, thus allowing penetration of the nanoparticles through the cell membrane [12]. Interestingly, Giordano et al. showed that electrochemical procedures may promote the formation of anatase, and high voltage anodization treatments promote osteoblasts and fibroblasts proliferation [42].

It is increasingly important for the biocompatibility of biomedical devices to study how the surface chemistry, morphology and nanotopography affect the adhesion process of the proteins. It is important to compare experimental results [43] and theoretical studies about the protein adsorption process, considering for example the same protein and as substrate different hydrophobic or hydrophilic, flat or curved surfaces. About twenty years ago, I began modeling the adsorption process of an albumin subdomain on ordered hydrophobic graphene-like surfaces with different curvature or chirality, such as graphite or achiral and chiral single-walled carbon nanotubes (SWCNT), or the adsorption in the inner and outer carbon nanotubes surfaces at different curvature and on hydrophilic amorphous polymeric polyvinyl alcohol (PVA) surface [44–48]. These theoretical studies have shown their importance for understanding the phenomena of protein adsorption on the surfaces of biomaterials with interesting comparison with experimental data.

Protein adsorption plays a key role for the continuous dialogue with the biological environment. In many cases, biomaterials get into direct contact with blood. Human serum albumin (HSA) is the most abundant blood protein. HSA is in general a soft protein. Experimentally it was found that after immobilization or adsorption on TiO_2 surfaces [49] this soft blood protein undergoes conformational changes induced by the surface topography affecting also its tertiary structure, then the functionality [50–58]. These studies confirm the importance not only of the similar surface chemistry of TiO_2 surfaces but also the influence of the surface curvature on the protein–biomaterial interaction process. Possible conformational changes can take place after adsorption depending on the curvature of the specific solid surface [44]. Bulk properties and surface properties, order or disorder and wettability can play an important role and they must be better investigated

also theoretically in order to better highlight the key factors for conformational changes, denaturation or reversible adsorption–desorption process [57–64]. Atomistic simulations can be a useful tool to describe well the surface chemistry and particular nanotopography of different crystallographic faces.

The theoretical study of albumin fragment adsorption on biomaterial surfaces at atomistic level was started by considering HSA subdomains [65,66]. Using the same methodology, it was found that on different TiO_2 polymorphs [67], the initial and final interaction energy and conformational changes are different for different titania polymorphs, but the key of the different interaction and conformational changes highlights that it is due to different particular surface chemistry considered. In fact, similar surface chemistry of specific crystalline face of different polymorphs can exhibit similar interaction and protein adsorption process.

It is crucial to focus the attention at atomistic level on the microscopic properties in order to better understand the macroscopic ones. The aim of this work is the theoretical study and characterization of HSA in terms of the interaction strength and conformational changes in the secondary and tertiary protein structure after the physisorption and competitive surface adsorption on TiO_2 anatase crystalline faces and its 3D-nanosized crystal. In particular, in order to study how the adsorption process of organic molecules can change considering different crystallographic faces of same TiO_2 polymorph, in particular the anatase, I began a theoretical study considering the quinoline molecule [68,69]. Quinoline molecules are much smaller with respect to the HSA subdomain studied in previous theoretical work. Using molecular mechanics (MM) and molecular dynamics (MD) methods I tried to understand the role of topography effects, how it is important for competitive adsorption both on different single TiO_2 anatase crystallographic faces separately considered. In particular, the TiO_2 anatase hydroxylated (0 0 1) face, the (1 0 0), the (0 0 −1) and the (1 0 1) faces and an ideal TiO_2 anatase nanosized crystal formed also by three of these different faces; in this case the (0 0 1), the (1 0 0), and the (0 0 −1) facets were studied. In the literature, Mashatooki et al. investigated the interaction between a potential anticancer RNA aptamer and TiO_2 anatase (1 0 1), (1 0 0) and (1 1 0) crystallographic faces, confirming how particular crystallographic faces can influence the adsorption process [70]. Interestingly, Yan et al. investigated how concentration-dependent diffusion is central in the accurate regulation of a desirable ratio of TiO_2 mixed anatase facets when growth of an anatase crystal itself occurs, indicating that facet engineering highlights the fundamental understanding of kinetic growth of facets with capping agents [71]. The basic function of a capping agent is realized by preferential binding on a certain facet using its functional groups. Additionally, the proteins may be capping agents for this kind of study, but the simulations considering them at different concentration are very time-consuming due to the larger number of atoms in proteins or its fragments.

In the present work the idea to start the competitive adsorption process on an ideal TiO_2 anatase 3D-nanocrystal is also reported, compared with the adsorption on single facets separately considered to have a larger surface area. Furthermore, the dimension of the specific facet influences the strength of the possible protein–biomaterial non-covalent interactions, and then the conformational changes and possible spreading are more evident in the final tertiary structure, that is, the structure affecting the final functionality of the protein adsorbed on solid surface.

2. Materials and Methods

This theoretical study is based on molecular mechanics (MM) and molecular dynamics (MD) simulations. All MM and MD simulations were performed with Materials Studio, Discovery Studio packages and Analysis Module in InsightII/Discover program (Accelrys Inc., San Diego, CA, USA) [72,73]. Using the same simulation protocol proposed in previous work all calculations are performed with COMPASS force field [74], with a Morse potential for the bonded atoms, in implicit water using a distance-dependent dielectric constant and by keeping fixed all the TiO_2 atoms [67,68]. Different facets of crystalline TiO_2 anatase were

prepared from the available templates in module Builder in Materials Studio packages containing the structure of pure anatase and the lattice parameters of the original crystal unit cell $a = b = 3.776$ Å, $c = 9.486$ Å, $\alpha = \beta = \gamma = 90°$. The size of the TiO_2 anatase surfaces studied both for the (0 0 1) and the (0 0 −1) face is equal to 11.3 Å × 56.6 Å × 85.4 Å multiplying the crystallographic axes *a*, *b*, *c* by 3, 15, 9, respectively. For the (1 0 0) TiO_2 crystallographic face the dimension of the solid surface is equal to 90.6 Å × 67.9 Å ×18.9 Å multiplying the *a*, *b*, *c* crystallographic axes by 24, 18, 2, respectively. Finally, the exposed surface of the (1 0 1) crystallographic face, built using Materials Studio packages (Build, Cleave Surface), is equal to 95.0 Å × 65.0 Å. The ideal TiO_2 anatase 3D-nanosized crystal was modelled with an idealized shape, multiplying the crystallographic axis *a*, *b*, *c* by 15, 15, and 6, respectively, forming a cubic-shaped nanocrystal of side equal to 57.0 Å.

The coordinates of HSA fragment (human serum albumin (HSA), 1AO6 [74]) were taken from the experimental results obtained by single-crystal X-ray analysis and deposited with the Protein Data Bank (PDB). The fragment protein is considered charged at physiological pH = 7.4 using Biopolymer module of InsightII/Discover [72]. The HSA subdomain, its structure and hydropathy are described in detail in previous work [65].

All energy minimizations were carried out up to an energy gradient lower than 4×10^{-3} kJ mol^{-1} Å^{-1}. The MD simulations were performed at a constant temperature (300 K), controlled through the Berendsen thermostat. Integration of the dynamical equations was carried out with the Verlet algorithm using a time step of 1 fs, and the instantaneous coordinates were periodically saved for further analysis or geometry optimization. The MD simulations lasted 10 ns for the adsorption on the different TiO_2 anatase surfaces, and 30 ns when the competitive adsorption on the ideal 3D nanocrystal was considered (see Section 3.2). Within the MD runs, the time changes of the total and potential energy together with its components, in particular the van der Waals contribute, were monitored using the module Forcite in Materials Studio packages. In general, these quantities showed an initial large decrease, and then fluctuated around a constant value, indicating achievement of equilibrium or of a stable adsorption state that present slow conformational changes after maximizing the interaction with the anatase surface. The conformational analysis (radii of gyrations, R_g, and solvent-accessible surface area, SASA) was made using Discovery Studio packages. The subset of amino acids within 6 Å from the solid surface was defined by atoms near the surface within 6 Å and then counting all different specific amino acids in contact with the surface, as in previous work about the adsorption on TiO_2 polymorphs [67].

All simulations in the last twenty years have been performed at temperature equal to 300 K. Often in literature, room temperature or 300 K is the temperature of the MD runs, the temperature of the adsorption process of protein on solid surface, not the body temperature. It will be possible to start the same simulations at body temperature (which incidentally is higher than 300 K by only a few degrees), in order to study the interaction strength and possible conformational changes of protein in an adsorption process on the solid surface at this specific temperature.

3. Results and Discussion

This theoretical study is based on the simulation protocol for protein adsorption on biomaterial surfaces proposed in previous work [19–22,65] that involves three sequential steps:

(i) at first, the initial energy minimization considering different initial trial geometries of interaction albumin fragment-specific solid TiO_2 surface (see Section 3.1.1);
(ii) the MD runs at constant temperature until the potential energy, the van der Waals contribute and the conformational changes achieve an equilibrium state, starting from both the initial geometry with the lowest potential energy and the initial metastable geometry displaying the highest initial potential energy (see Section 3.1.2);
(iii) the final geometry optimizations of the final configuration assumed by the adsorbed protein fragment at the end of the MD run (see Section 3.1.2).

Steps (i) and (iii) respectively yield the initial and the final adsorption optimized geometries.

The adsorption on TiO_2 anatase 3D-nanocrystal is reported in the Section 3.2. In this case, three albumin *A*-subdomains are initially placed near three different TiO_2 anatase facets of the ideal 3D-nanocrystal and a MD run lasting 30 ns is performed. In the next sections, all results are presented and discussed.

3.1. Adsorption of HSA Fragment on Different TiO_2 Crystallographic Anatase Faces

Using theoretical methods based on molecular mechanics (MM) and molecular dynamics (MD) simulations, the interaction between HSA *A*-subdomain and both single different crystallographic faces and three dimensional (3D) ideal nanocrystal of TiO_2 anatase were investigated.

The four different crystallographic TiO_2 anatase faces studied in this work are reported in Figure 1 panels (a–c), together with a model of a nanosized crystal (panel d). The (0 0 1) TiO_2 anatase surface exposes hydroxyl groups, the (0 0 −1) TiO_2 facet exposes titanium atoms, the (1 0 0) TiO_2 surface exposes both titanium atoms and bridging oxygen atoms; the (1 0 1) TiO_2 anatase face exposes hydroxyl groups, titanium atoms and bridging oxygen atoms. The albumin fragment studied in previous work [65] at physiological pH is reported in panel (e). This fragment is composed by three α-helices A1A, A2A, A3A connected as in the chemical structure reported in PDB [74]. At first, in Section 3.1, this HSA fragment will interact separately with the individual four crystallographic surfaces reported in panels (a–c) mentioned above. In the second step, in Section 3.2, the protein fragment adsorption will be considered on a model 3D nanocrystal of anatase exposing the three (0 0 1), (0 0 −1) and (1 0 0) faces, as previously studied about competitive adsorption of small quinoline molecules important for a photocatalytic activity [68,69].

3.1.1. Initial Adsorption on Different TiO_2 Anatase Faces

The initial adsorption was simply modeled by energy minimization of the protein placed close to the selected surfaces as described at the beginning of Section 3.

In Figure 2, the initial most stable optimized geometries after MM calculation for the four TiO_2 anatase crystallographic surfaces are reported. In all geometries the secondary structure changes in order to maximize the interaction with the specific TiO_2 solid surface. For all initial energy minima, the interaction energy, E_{int}, and the strain energy, E_{strain}, were calculated [65–67].

The interaction energy is defined as $E_{int} = (E_{free} + E_{TiO2\ anatase\ face}) - E_{tot}$. In all simulations the anatase surface atoms are kept fixed, as just considered for all atoms of solid surfaces studied in the adsorption process of the same HSA fragment on graphite, SWCNTs surfaces [44,45]. Then, $E_{TiO2\ anatase\ face} \equiv 0$, although of course all TiO_2 atoms do correctly interact with the HSA subdomain. The E_{free} is the potential energy of the free, isolated native subdomain in the optimized geometry. According to this definition, the E_{int} value corresponds to the energy released upon adsorption due to favorable interaction with the solid surface. Instead, $E_{int} > 0$ is the energy cost to detach the protein fragment favorable adsorbed on the surface, while the energy released upon adsorption is given by $-E_{int}$ (i.e., with the opposite sign).

The strain energy is defined as $E_{strain} = E_{frozen} - E_{free}$, where E_{frozen} is the energy of the isolated HSA *A*-subdomain in the frozen minimized geometry they adopt upon adsorption. This interesting energy contribute explains the energy cost for the albumin fragment to maximize the favorable interactions with the solid surface breaking the hydrogen bonds (H-bond) and the other intramolecular interactions in the native conformation.

When the interaction energy is more favorable, more conformational changes near the surface occur in order to optimize the favorable adsorption process. Whereas, when the initial interaction energy is less favorable and some H-bonds between protein fragment and the atom exposed by the surface are possible, fewer protein conformational changes take place [65,66]. It will be interesting to understand how different topographies and exposed

atoms can induce different behavior and different intrinsic energy, $E_{intrinsic}$, calculated as the interaction energy normalized by the number of residues in contact with the anatase surface [67]. Additionally, the nature of amino acids in contact with the surface, thanks to their more or less hydrophobic or hydrophilic nature, can influence the strength of the interaction, then, the final tertiary structure of protein.

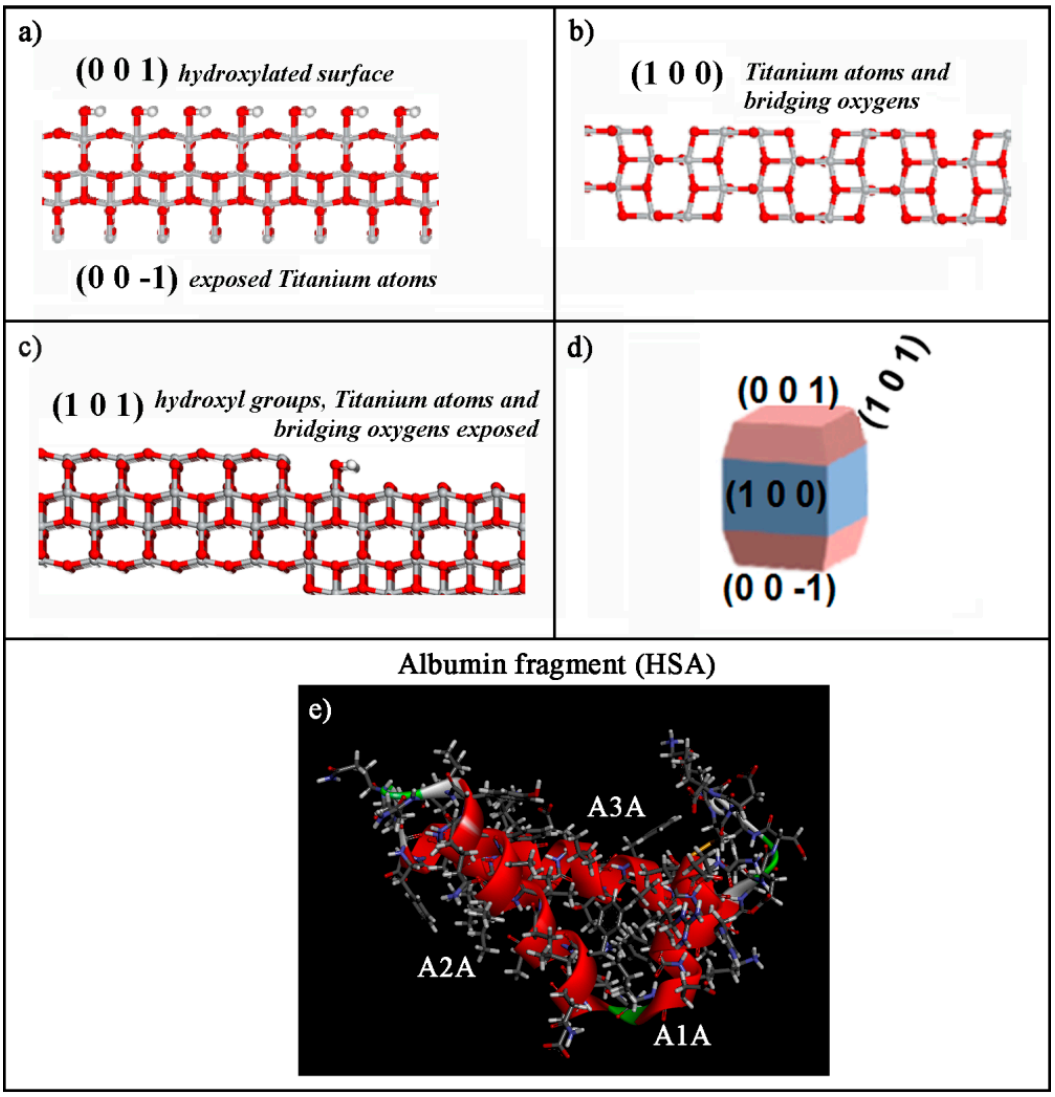

Figure 1. In panels (**a**–**c**) the modeled TiO_2 anatase surfaces are shown. In panel (**a**) both the (0 0 1) and (0 0 −1) crystallographic faces are reported, while in panels (**b**,**c**), the (1 0 0) and (1 0 1) surfaces are reported, respectively. The color code is the following: the oxygen atoms are in red, the titanium atoms in grey, nitrogen atoms in blue, carbon atoms in dark grey, hydrogens in white. Panel (**d**) shows the scheme of a 3D ideal TiO_2 anatase nanocrystal with all the different crystallographic faces indicated. In panel (**e**), the human serum albumin (HSA) fragment is reported. For the albumin fragment the carbon atoms are in dark grey, the nitrogens in blue, the oxygens in red, the hydrogens in white. In the secondary structure, the backbone in α-helix is in red ribbon, the random coil strands are reported in grey, while the turns are in green.

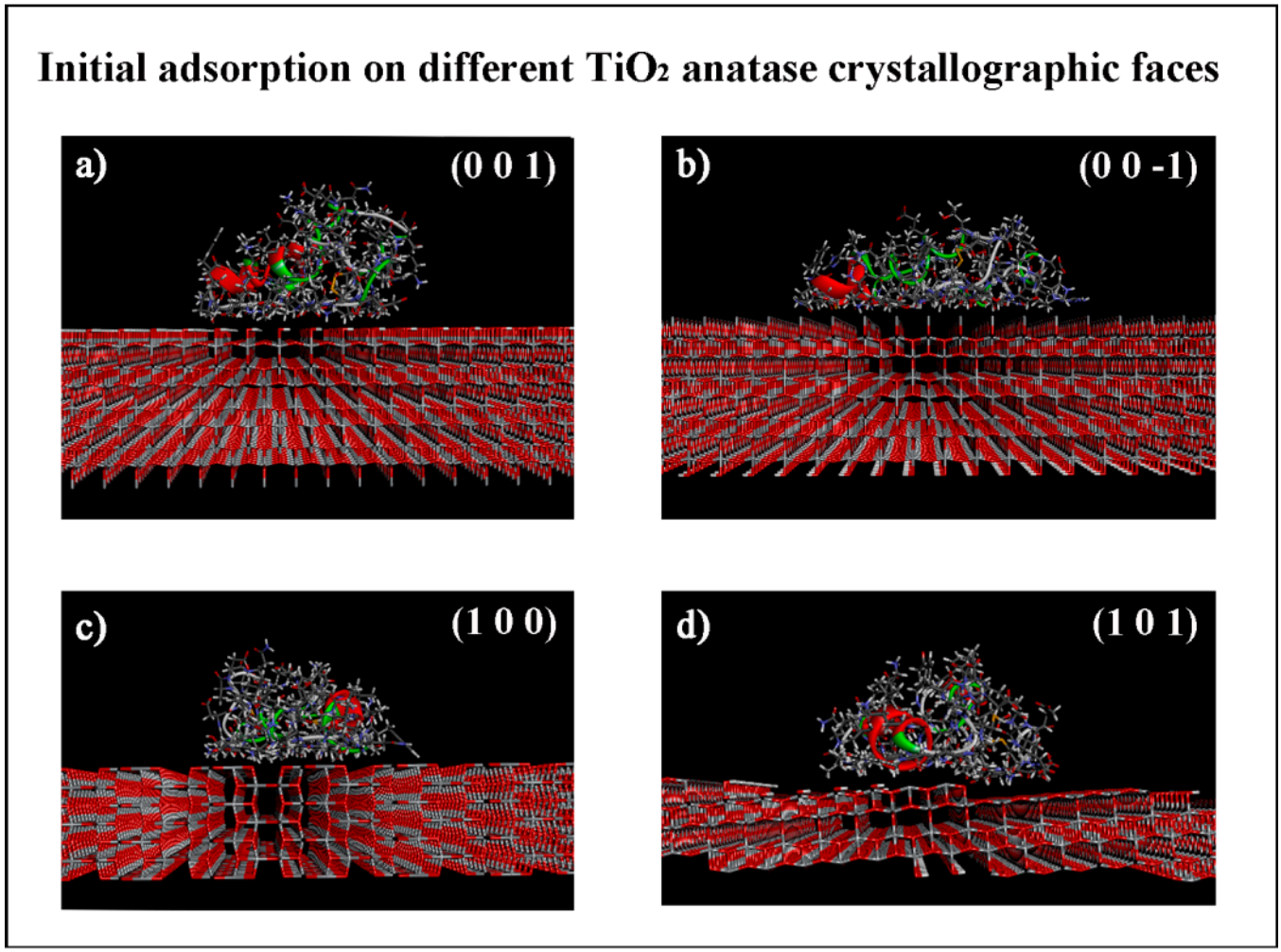

Figure 2. The initial most stable optimized geometries after molecular mechanics (MM) calculation for the four TiO_2 anatase crystallographic surfaces considered, the (0 0 1), (0 0 −1), (1 0 0), (1 0 1) facets in panels (**a**–**d**), respectively, are reported. In particular, in panel (**c**), the initial optimized geometry is the same geometry as reported in previous work [67], shown here for comparison. For the color code, see Figure 1.

Both the protein–surface interaction energy and the conformational changes that take place in the initial adsorption state were studied for all different initial trial geometries (see Figure S1) of HSA *A*-subdomain near the four different crystallographic faces reported in Figure 1. Some residues display an α-helix in the secondary structure as in the native state. Interestingly, again a linear dependence was found between the interaction energy and the number of amino acids in contact with the TiO_2 anatase facets as found in previous work [67].

The initial energy minima provide also an estimate of the interaction strength through the number of amino acids in contact with the surface, with interesting comparison with data just published both on TiO_2 polymorphs and also on hydrophobic graphite surface and carbon nanotubes and on hydrophilic surfaces such as amorphous poly(vinyl alcohol) surface. In Figure 3, the interaction energy and the strain energy are reported as a function of the number of the amino acids in contact with the surface at a distance of less than 6 Å.

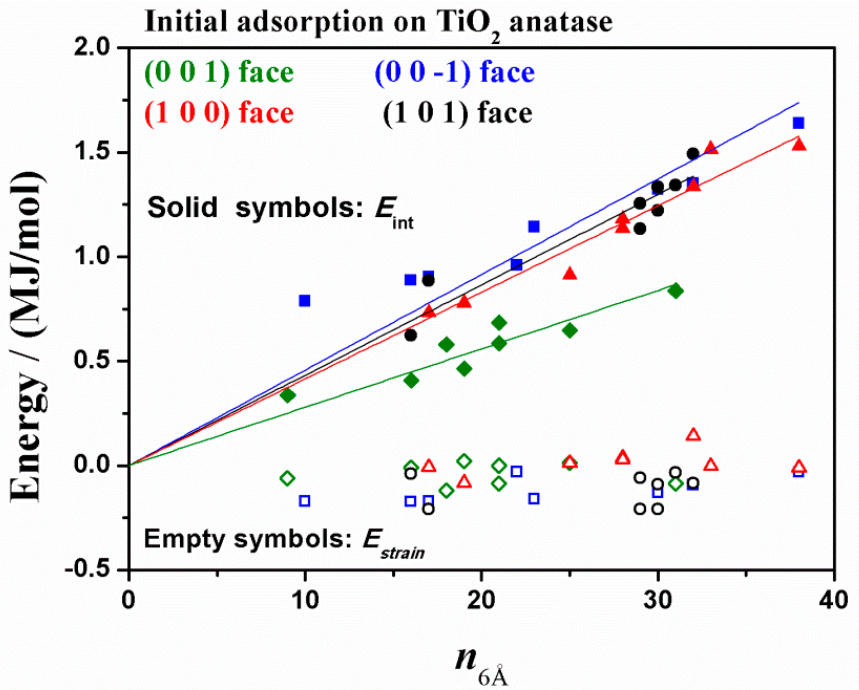

Figure 3. The initial interaction energy between HSA subdomain calculated on different crystallographic TiO_2 surfaces (solid symbols) and the strain energy (empty symbols) plotted as a function of the number of amino acids in contact with the TiO_2 anatase surface within 6 Å. These values are calculated for all the different initial geometries reported in Figure S1 considering all four TiO_2 crystallographic anatase faces reported in Figure 1. Color code: in green, in blue, in red and in black, respectively, the values calculated for the (0 0 1), the (0 0 −1), the (1 0 0) and the (1 0 1) crystallographic surface. The common best-fit lines through the origin for the only E_{int} values are reported and given by Equations (1)–(4).

Taking into account the different starting orientations of the protein subdomain producing different optimized adsorption geometries corresponding to a local energy minimum, E_{int} turns out to be linearly correlated with the number of amino acids that are in contact with the surface as in previous work about the adsorption of the same HSA fragment on graphite [65,66], SWCNT [44], PVA surface [48]. $n_{6Å}$ is the number of amino acids in contact with the surface, where 6 Å is conveniently taken as the upper distance for a contact interaction as reported in previous work about the adsorption on TiO_2 rutile, anatase and brookite [67]. The linear dependence, due to the additive nature of the attractive interactions, shown in Figure 2 together with the best-fitting lines through the origin, is given by:

$$E_{int} = (28.0 \pm 1.1) \times n_{6Å} \text{ kJ/mol on } TiO_2 \text{ anatase (0 0 1) face } R^2 = 0.987 \quad (1)$$

$$E_{int} = (45.8 \pm 2.3) \times n_{6Å} \text{ kJ/mol on } TiO_2 \text{ anatase (0 0 } -1\text{) face } R^2 = 0.980 \quad (2)$$

$$E_{int} = (41.5 \pm 1.0) \times n_{6Å} \text{ kJ/mol on } TiO_2 \text{ anatase (1 0 0) face } R^2 = 0.995 \quad (3)$$

$$E_{int} = (43.3 \pm 1.2) \times n_{6Å} \text{ kJ/mol on } TiO_2 \text{ anatase (1 0 1) face } R^2 = 0.993 \quad (4)$$

The simulation results of the initial adsorption stage on the isolated surfaces indicate a less favorable interaction with the TiO_2 (0 0 1) surface, the most hydrophilic crystallographic face having hydroxylated groups exposed; the adsorption on the crystallographic (0 0 −1) face display the most favorable interaction strength, while the adsorption on TiO_2 anatase (1 0 1) face and on (1 0 0) face show a similar, favorable behavior.

As for the strain energy, it is interesting to note that for all initial geometries considered for the (1 0 1) and (0 0 −1) surface, all strain energy values are negatives, for the (0 0 1) six geometries, the E_{strain} values are negative. For the (1 0 0) surface, some geometries have positive values, while other ones have some negative values. As found about the

adsorption on TiO_2 polymorphs [67], a linear dependence between the strain energy and the number of amino acids in contact with the surface was not found. Regardless, in keeping with previous results, it was found that the strain energy is always lower than the interaction energy, suggesting possible conformational changes at room temperature in order to maximize the favorable interaction with the titania surfaces.

In Figure 4 an interesting comparison is shown regarding the theoretical results of the adsorption process of HSA *A*-subdomain calculated only on TiO_2 anatase (0 0 −1) and the (0 0 1) crystallographic facets, and the theoretical results reported in my previous work of HSA and fibronectin subdomains with an unlike secondary structure on hydrophobic graphite and on hydrophilic PVA, and of the HSA *A*-subdomain on external surface of SWCNT at different curvature. The TiO_2 anatase (0 0 −1) face exposing titanium atoms displays a favorable interaction with albumin fragment, while the TiO_2 anatase (0 0 1) face exposing more hydrophilic hydroxyl groups displays a less favorable interaction, similar to that exhibited by the same fragment on amorphous PVA.

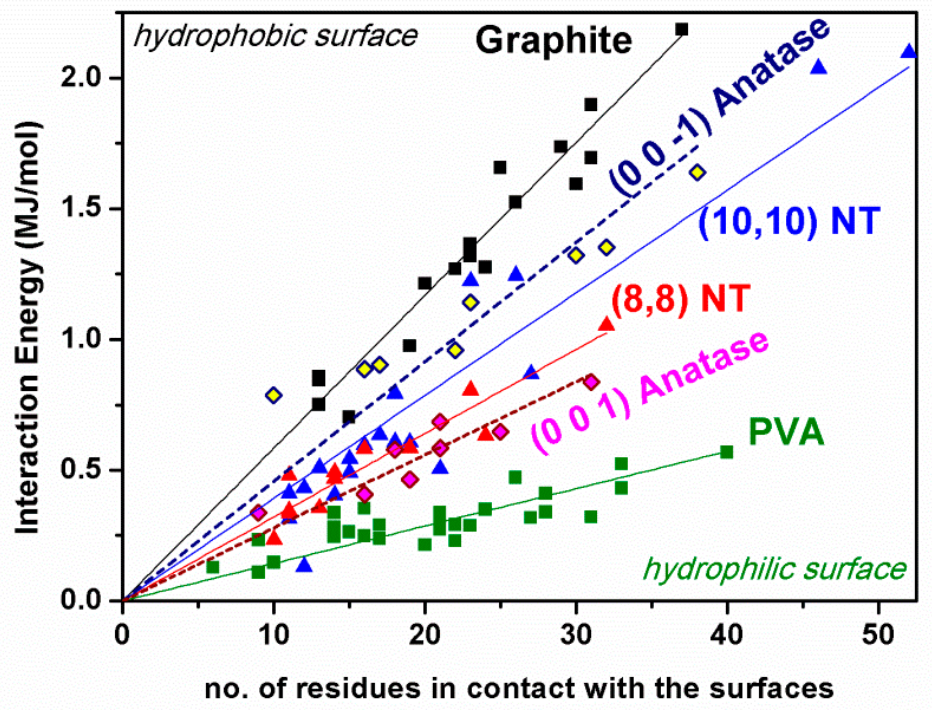

Figure 4. The initial interaction energies calculated as a function of the number of residues in contact with the external surfaces in the initial geometries reported in Figure S1 considered for different materials: the hydrophobic flat graphite surface (black symbols, for two albumin subdomains and fibronectin modules [65,75]), external surface of the hydrophobic curved (10,10) and (8,8) SWCNT surfaces (blue and red symbol respectively, calculated for the *A*-subdomain [44]), hydrophilic amorphous PVA surface (green symbols, for albumin subdomains and fibronectin modules [48]) and the two TiO_2 crystallographic anatase faces studied in present work, in particular the (0 0 −1) in yellow symbols and the more hydrophilic (0 0 1) face in fuchsia symbols. The common best-fit lines through the origin for the only E_{int} values are reported.

It is important to highlight that the results obtained in the first theoretical work [65] using the Consistent Valence Force Field (CVFF) considering the albumin *A*-subdomain and graphite surface are also obtained using the COMPASS force field, that is well parametrized for the graphite surface and TiO_2 anatase surface here studied, thus confirming both the initial and final albumin fragment conformational changes and the strength of the interaction. Therefore, the comparison in Figure 4 for results obtained using these different force fields is not only qualitative but also quantitative.

In the next section, the results obtained at the end of MD run starting from both the more and the less stable geometries calculated for all four TiO_2 anatase faces are reported and discussed.

3.1.2. Final Adsorption on Different TiO_2 Anatase Faces

After a MD runs lasting 10 ns starting from the less stable and the most stable initial geometries calculated in the initial interaction stage on single TiO_2 anatase crystallographic faces and after energy minimization of the final conformation assumed by the albumin *A*-subdomain the final optimized geometries are studied (see Figures 5 and 6). As found on graphite surface [63,74] and on amorphous PVA [48], in most cases, the tendency of this soft protein is to maximize the interaction with the surface overcoming the energy barrier due to conformational changes in the secondary structure.

After adsorption, the increased favorable interaction with TiO_2 surfaces induce a formation of a monolayer of amino acids in contact with the surface with part of backbone in ordered parallel strands [64,67]. In particular, on the hydroxylated TiO_2 anatase (0 0 1) surface numerous H-bonds are formed with the surface, then the surface coverage is relatively less extended thanks to the H-bonds in contact with the surface (see Figure S2) that prevents the full surface spreading and stabilize the adsorbed protein conformation. On the three other TiO_2 crystallographic facets, the formation of a monolayer of amino acids is observed near the surface (see Figure 5), forming very few or no H-bonds with the surface (see Figure S2).

The HSA *A*-subdomain exhibits an extensive nanopatterning with the protein backbone in parallel strands and some hairpin arrangements as they are found on the more hydrophobic surface such as graphite and SWCNTs.

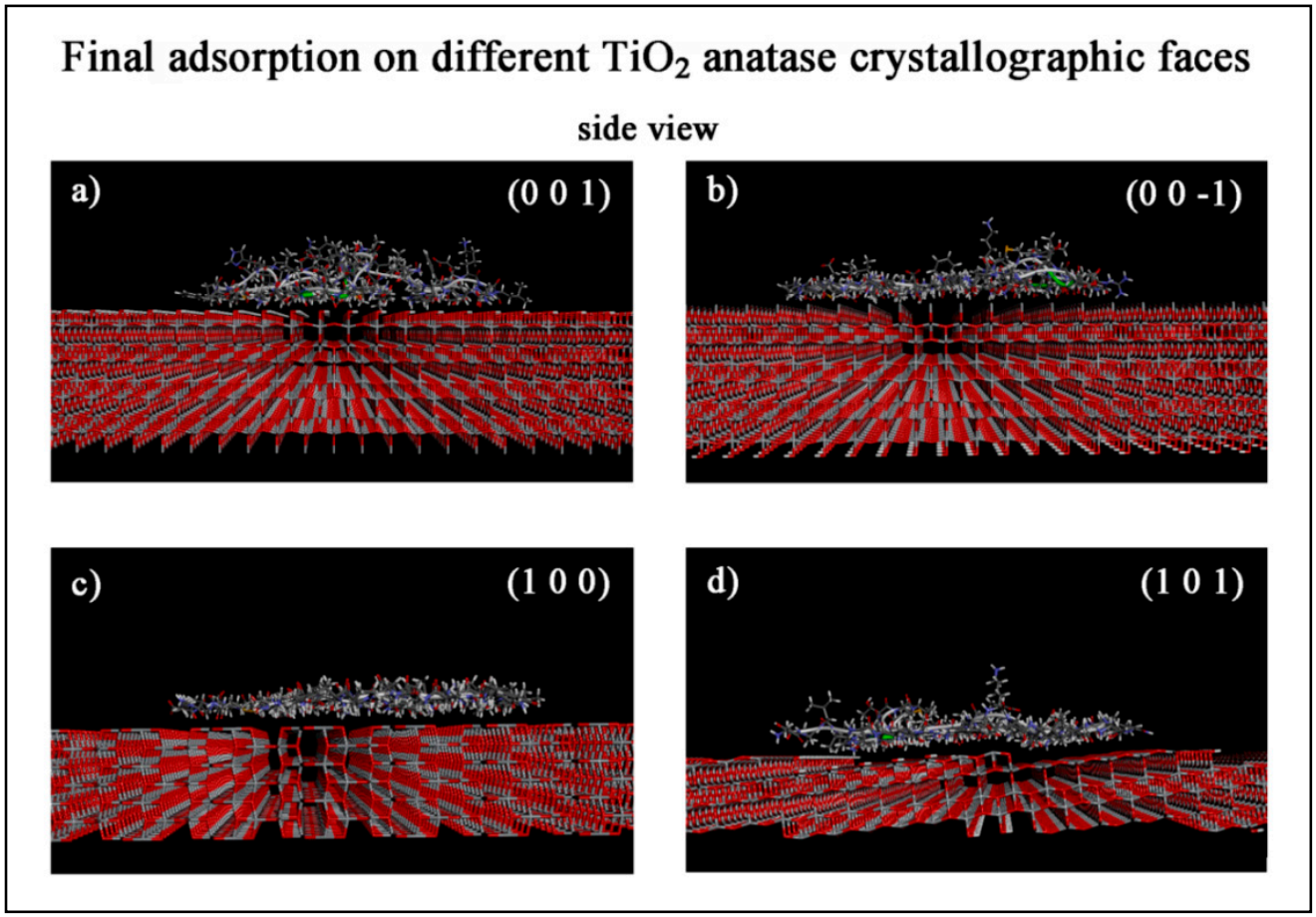

Figure 5. Side view of the final most stable optimized geometries after a MD run lasting 10 ns of the albumin *A*-subdomain adsorbed on the four TiO_2 anatase crystallographic surfaces considered, the (0 0 1), (0 0 −1), (1 0 0), (1 0 1) faces in the panel (**a**–**d**), respectively. For the color code, see Figure 2.

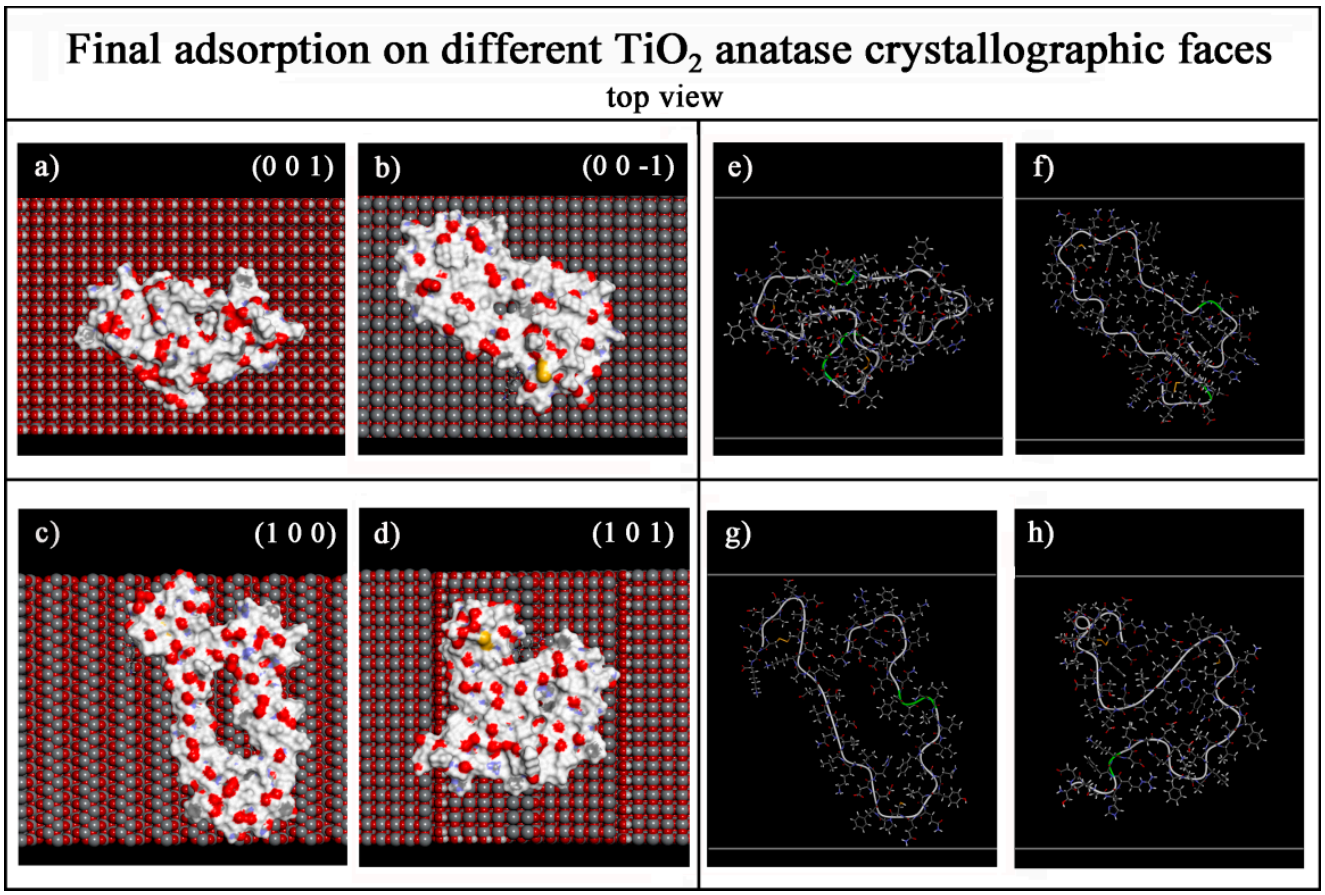

Figure 6. Top view of the final most stable optimized geometries after MD run lasting 10 ns of the albumin fragment adsorbed on TiO_2 anatase crystallographic (0 0 1), (1 0 −1), (1 0 0), (1 0 1) faces in panels (**a**–**d**) respectively on the left. In particular, the surface atoms are in space-filling CPK representation and the top view of the albumin fragment adsorbed represents the surface area accessible to the solvent, colored by atoms. In panels (**e**–**h**) at right only the atoms and the secondary structure of albumin adsorbed *A*-subdomain are reported. For the color code, see Figure 2.

Both the interaction and the strain energy values calculated in the initial and in the final adsorption stage for the most stable and the less stable optimized geometries shown in Figure 5 are reported in Tables 1 and 2, respectively, together with the final intrinsic energy, the radius of gyration, the volume occupied and the solvent-accessible surface area of the adsorbed HSA *A*-subdomain. Figure S3 reports the Ramachandran plots of the albumin fragment in the four most stable final adsorption state near all four TiO_2 anatase faces shown in Figure 5. In these plots, the values of dihedral angles Ψ and Φ are similar to disposition of backbone in parallel strand as found on TiO_2 polymorphs [67]. In the final adsorption state, all three α-helices are disrupted in order to maximize both the interaction with the solid surface and intramolecular interactions with strands of backbone, now in a parallel arrangement.

Table 1. The initial and final E_{int} and E_{strain} values, final values of the intrinsic energy, $E_{intrinsic}$, of the radius of gyration (R_g), of the volume occupied and of the solvent-accessible surface area (SASA) calculated for the HSA fragment after MD run in the most stable geometries found on the four specific TiO_2 anatase faces.

TiO_2 Anatase Crystallographic Face	*Initial* E_{int} (kJ/mol)	E_{strain} (kJ/mol)	*Final* E_{int} (kJ/mol)	E_{strain} (kJ/mol)	$E_{intrinsic}$ (kJ/mol)	R_g (Å)	Volume (Å^3)	SASA (Å^2)
(0 0 1)	837.6	−86.3	2000.0	−561.6	54.1	14.2	7133	3699
(0 0 −1)	1639.2	−32.7	2738.5	−104.4	54.8	20.0	7055	4541
(1 0 0)	1529.8	12.2	3103.0	228.0	51.7	21.3	6854	5005
(1 0 1)	1491.2	−84.3	2861.2	−8.158	54.0	17.6	6961	4613

Table 2. The initial and final E_{int} and E_{strain} values, final values of the intrinsic energy, $E_{intrinsic}$, of the radius of gyration (R_g), of the volume occupied and the solvent-accessible surface area (SASA) calculated for the HSA fragment after MD run in the less stable geometries found on the four specific TiO_2 anatase faces.

TiO_2 Anatase Crystallographic Face	*Initial* E_{int} (kJ/mol)	E_{strain} (kJ/mol)	*Final* E_{int} (kJ/mol)	E_{strain} (kJ/mol)	$E_{intrinsic}$ (kJ/mol)	R_g (Å)	Volume (Å^3)	SASA (Å^2)
(0 0 1)	336.6	−60.6	1959.8	−578.7	56.0	13.5	7433	3466
(0 0 −1)	787.2	−173.0	2574.4	−311.4	59.9	15.4	7290	3873
(1 0 0)	731.2	−7.98	2716.0	−209.5	59.0	15.1	7127	4060
(1 0 1)	622.4	−39.8	2853.0	−75.65	54.9	16.8	7012	4506

Interestingly, the larger interaction energy and larger radius of gyration are calculated after adsorption on TiO_2 anatase (1 0 0) facet, displaying larger spreading due to favorable interaction with the surface. Moreover, a positive E_{strain} value indicates the energy cost to disrupt the intramolecular H-bonds of the protein fragment in the native state. In the other three different optimized geometries, the new arrangements assumed by protein fragment near the surface display a more stable conformation with respect to the native state with the backbone in ordered parallel strands following the nanotopography of the surface. In the adsorbed final conformation, all or almost all amino acids are in contact with the surface. Larger values of $E_{intrisic}$ are calculated for the final less stable optimized geometries indicating very similar value for the (1 0 1), (1 0 0) and (0 0 −1) faces, a lower value is calculated for the TiO_2 anatase (0 0 1) facet that displays lower R_g, therefore a smaller spreading on the surface. Near the surface, all hydrophilic and hydrophobic residues are in contact with the surface, and not only the residues that best interact with this specific hydroxylated crystalline surface, because of the topological connectivity [75]. In the less stable final geometries, all E_{strain} values which are negative indicate a new stable conformation of HSA *A*-subdomain near anatase surface. Barinov et al. [76] reported that hydrophobic Highly Oriented Pyrolytic Graphite (HOPG) surfaces induce conformational rearrangements in blood protein such as HSA, forming a layer of amino acids in contact with the flat graphite surface as indicated using AFM, whereas on HOPG surface covered by amphiphilic monolayer, the protein conformation remains more intact. In previous theoretical studies about the adsorption of the same HSA *A*-subdomain on PVA surface [48], the H-bonds between protein fragment and polymeric surface exposing hydroxyl groups prevent spreading on the surface, as it is found here after adsorption on the hydroxylated TiO_2 anatase crystalline (0 0 1) face.

The final theoretical results about the adsorption process on TiO_2 anatase 3D crystal are discussed in the next Section 3.2.

3.2. Adsorption on Ideal TiO_2 Anatase 3D Nanocrystal

In this section, the competitive adsorption process of HSA *A*-subdomain in TiO_2 anatase 3D nanocrystal just studied in a previous work [68] is described considering in particular three different crystallographic facets, namely, the TiO_2 anatase (0 0 1) face,

the (0 0 −1) face and four (1 0 0) faces (see Figure 7). These facets were simultaneously present considering the ideal TiO_2 anatase 3D-nanocrystal, in order to better understand the competitive protein adsorption process. In previous work the adsorption process of molecules smaller than the albumin fragment was studied, such as quinoline molecules considered at small and at large concentration. The MM and MD methods have been demonstrated to be a very useful tool to distinguish the influence in the adsorption process of the chemical structure and topography exposed by the specific crystallographic surface. In panels (a,b) of Figure 7, the initial geometry and the final optimized geometry obtained after a MD run lasting 30 ns are reported, respectively.

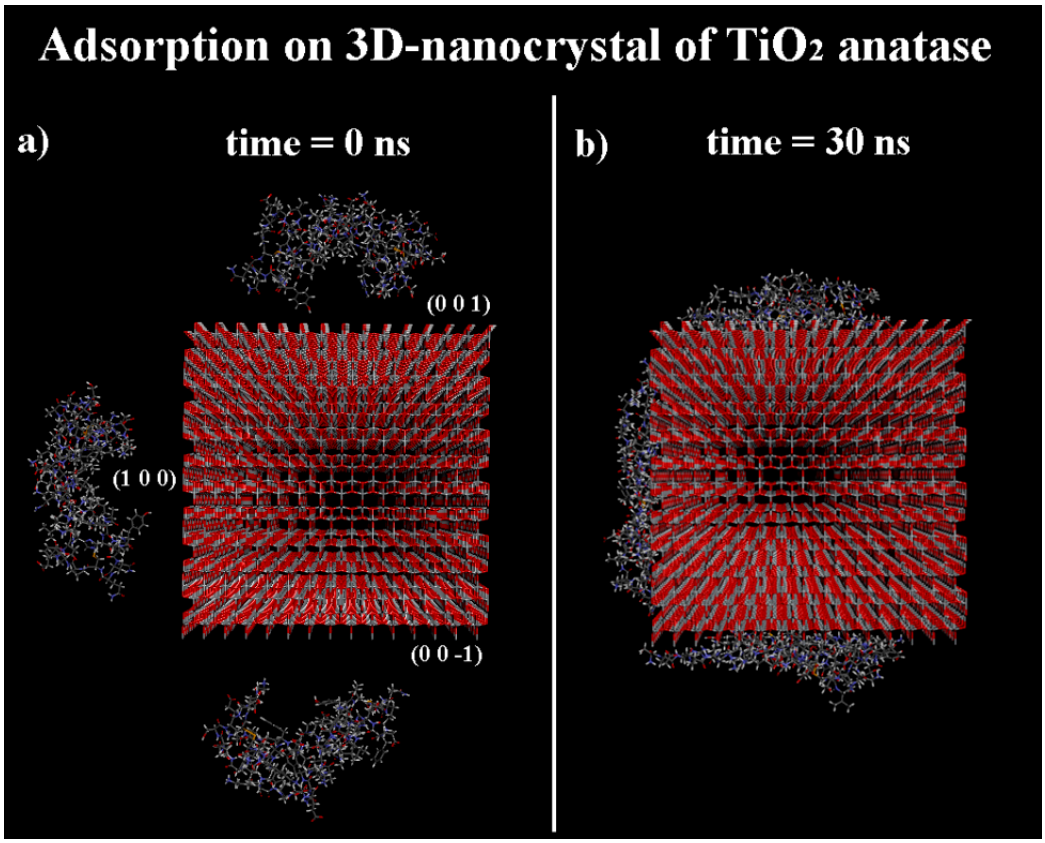

Figure 7. In panel (**a**) three albumin *A*-subdomains in the initial non-optimized geometry near the (0 0 1), (0 0 −1) and (1 0 0) TiO_2 anatase facets of the ideal 3D nanosized crystal, respectively on the top, on the left and at the bottom, are reported. In panel (**b**) the optimized system at the end of MD run lasting 30 ns is shown. See the color code in Figure 2.

The potential energy and the van der Waals contribution calculated during the MD run are reported in Figure 8.

At the end of the MD run, the optimized conformations of the three HSA *A*-subdomains adsorbed on three different TiO_2 anatase faces display fewer conformational changes with respect to those calculated after 10 ns on larger TiO_2 anatase surfaces (see values of the solid surface size in the Section 2 *Materials and Methods*). This fact is very important, as not only the specific surface chemistry of specific crystalline polymorphs exposed to the protein affects the adsorption process, but also the relative size of the crystalline facets considered with respect to the dimension of protein or its fragment. The surface size influences the adhesion process, in particular at longer time. The three different final optimized conformations of the HSA *A*-subdomains adsorbed on ideal TiO_2 anatase 3D nanosized crystal are reported in Figure 9. These conformations can be compared with the similar ones reported in Figure 6, related to the secondary structure of the albumin fragment calculated after the adsorption on single TiO_2 anatase facets. Table 3 reports the information about the

radius of gyration, the volume occupied together with the solvent-accessible surface area calculated at the end of MD run lasting 30 ns for the final optimized geometries shown in Figure 9.

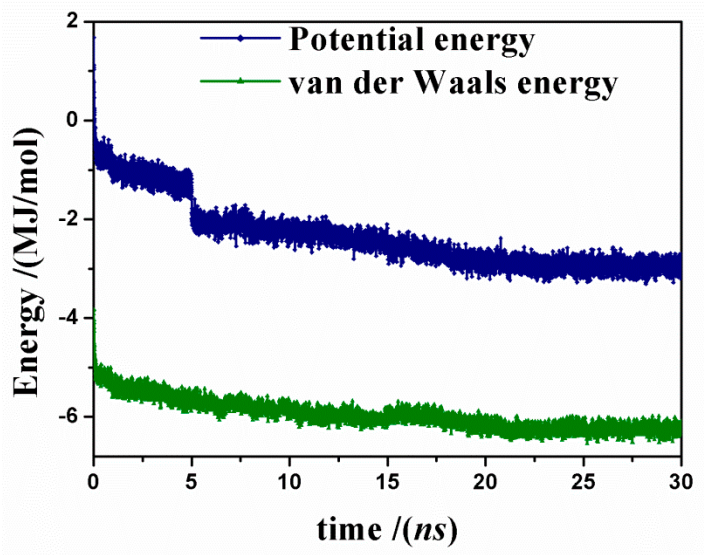

Figure 8. The potential energy (blue symbols) and the van der Waals contribution (green symbols) calculated during the MD lasting 30 ns at a temperature of 300 K.

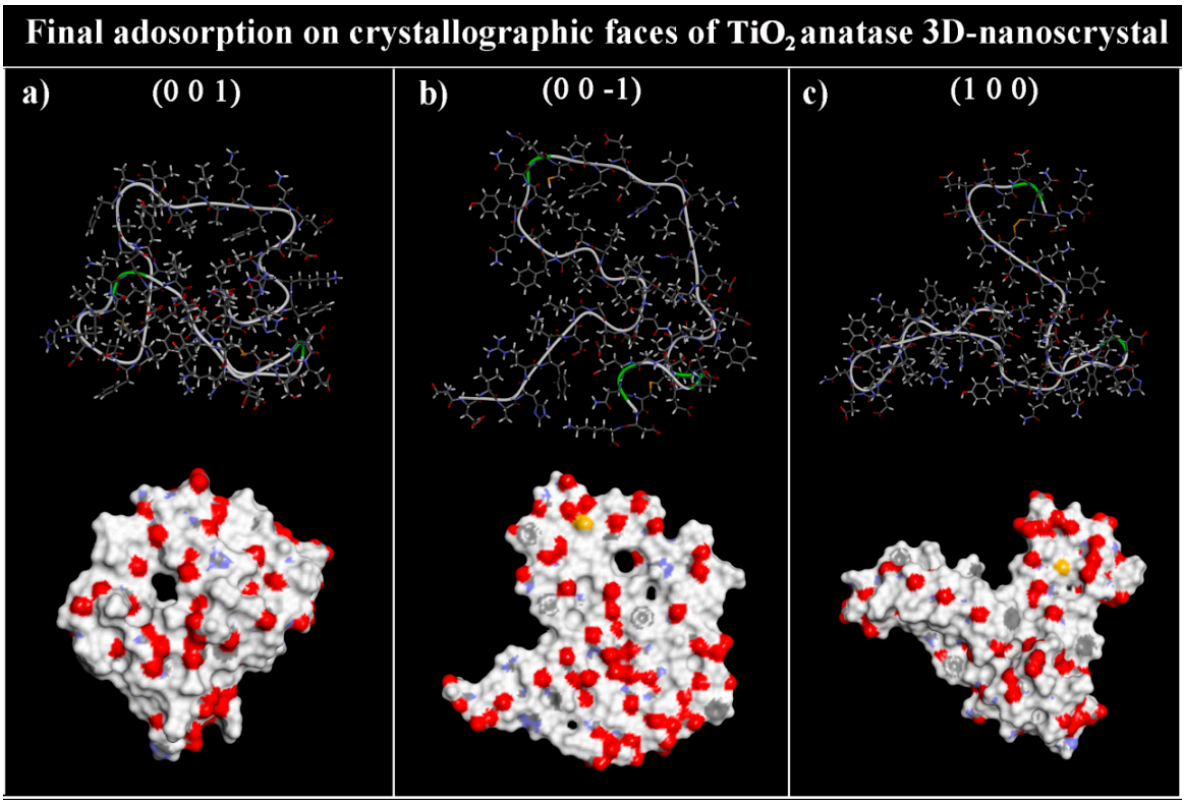

Figure 9. Final optimized geometries of HSA *A*-subdomain adsorbed on three TiO_2 anatase faces simultaneously present on the ideal TiO_2 anatase nanocrystal, in particular, the TiO_2 anatase (0 0 1), (0 0 −1) and (1 0 0) faces in panels (**a**–**c**), respectively. On the top, all atoms of HSA fragment with its secondary structure is reported. Bottom, the solvent-accessible surface area colored by atoms is reported. See the color code in Figure 2.

Table 3. Values of radius of gyration (R_g), the volume occupied and the solvent-accessible surface area calculated for by HSA fragment in the final adsorption stage after a MD run lasting 30 ns after the adsorption on specific TiO_2 anatase faces of the ideal TiO_2 anatase 3D nanocrystal.

Crystallographic TiO_2 Face	R_g (Å)	Volume (Å^3)	Solvent-Accessible Surface Area (Å^2)
(0 0 1)	13.7	7388	3668
(0 0 −1)	16.4	7053	4473
(1 0 0)	16.3	7137	4119

The radii of gyration values calculated on the more hydrophilic TiO_2 anatase (0 0 1) face after 10 ns on a separate surface and after 30 ns on the ideal TiO_2 anatase 3D nanocrystal are very similar (see Tables 2 and 3). The H-bonds with the anatase surface (see Figure S2 and Figure 9) stabilize the protein conformation yielding a smaller spreading on the surface, as found on hydrophilic amorphous PVA. Instead, larger radii of gyration are calculated after the MD run lasting 30 ns on TiO_2 (0 0 −1) and (1 0 0) facets of this ideal 3D anatase nanocrystal, displaying a minor surface coverage after the protein adsorption with respect to the same geometry calculated at the end of MD run on single crystalline surfaces separately considered. In particular, concerning the solvent-accessible surface area of the adsorbed protein fragment, the values calculated in the most stable geometries shown in Table 1, are similar in particular for the TiO_2 anatase (0 0 1) and (0 0 −1) faces, is smaller for the (1 0 0) face. In fact, in this case, less spreading takes place. Therefore, a good interaction energy and a smaller surface spreading of the adsorbed HSA *A*-subdomain are calculated in the final adsorption stage on the TiO_2 anatase 3D-nanocrystal having smaller surface size exposed to the albumin fragment.

In conclusion, the surface size can be very important in the adsorption process together with possible more or less favorable interaction when the interactions take place and a possible spreading process occurs during the time.

4. Conclusions

The surface chemistry, crystal structure, size and topography of the solid surface exposed to the biological environment influence the strength of the protein–biomaterial interactions and the possible conformational changes of proteins, hence the biocompatibility. Together with the strength of the interaction energy, the size of the surface on which the protein can adsorb, considered relative to both its overall shape in the native state and after the adsorption process, is an important factor that must be taken into account. In this theoretical work based on MM and MD methods using the simulation protocol proposed in previous studies about the adsorption process on hydrophobic graphene-like ordered surfaces [46,65] or hydrophilic amorphous PVA surface [48], and on TiO_2 polymorphs [67], the adsorption process of HSA *A*-subdomain is reported on both different crystallographic faces of TiO_2 anatase, as well as on its ideal 3D-nanosized crystal. Interestingly, it was found the most favorable initial interaction energy on the TiO_2 anatase (0 0 −1) crystallographic face which exposes titanium atoms, while a similar, though smaller, strength was calculated for the TiO_2 anatase (1 0 0) and (1 0 1) surfaces that expose titanium and bridging oxygen atoms, mimicking the similar behavior calculated for more hydrophobic curved SWCNTs surfaces. A weaker interaction energy with respect to the number of amino acids in contact with the surface was calculated for the hydroxylated TiO_2 anatase (0 0 1) face, exposing hydroxyl groups, displaying similar behaviors rather similar to that calculated for the hydrophilic polymeric amorphous PVA surface. In all these cases, in the initial interaction stage, some conformational changes in the secondary structure near the surface take place with local ordering. After performing the MD run, the protein well interacts with the TiO_2 anatase surface. As a result, the surface spreading of this soft protein and the surface coverage occur with extensive nanopatterning displaying the protein backbone in a parallel strand and some hairpin arrangements, similar to those found on ordered

hydrophobic crystalline graphite surface [44–46] by maximizing both intermolecular and intramolecular interactions.

Concerning the competitive adsorption on a TiO_2 anatase 3D-nanocrystal, after the MD run fewer conformational changes take place and the protein adsorption process is kinetically slower, than the previously studied larger separate crystalline TiO_2 faces. This result indicates that the size of the smaller exposed surface influence the protein–surface interaction, the possible surface spreading and coverage. Therefore, the size of the crystalline surface affects the kinetics of the protein adsorption process, the overall surface coverage and the possible surface spreading, producing a relatively more spherical and less flattened final protein structure.

In general, proteins or their fragments can be considered as a capping agent as well as small molecules at different concentration adsorbed on anatase surfaces [68] in order to kinetically control the growth mechanism and the fine-tuning of mixed facets on a single crystal increasing preferential facets on metal oxides. Then, the interaction energy and the surface covering of crystallographic TiO_2 anatase facets by proteins is an important aspect not only in order to better understand the protein interaction with the biological environment, hence the biocompatibility, but also from a technological point of view in order to promote the growth of one crystalline anatase surface over another. Combining experimental data and theoretical results describing at the atomistic level the protein and the specific surface chemistry, its nanostructure and topography, it will be possible to optimize the production of device composed preferentially by anatase and the enrichment of this specific TiO_2 polymorph structure more biocompatible.

It will be important to also study different metal oxides and, in general, new and interesting hybrid materials synthetized by sol–gel methods. In the last decade, not only titania surfaces but also different metal oxides have been studied as interesting materials for biomedical applications, such as ZrO_2, SiO_2 or ZnO, also as coating of titania surfaces. It will be important to continue the exploration of new hybrid materials in order to enhance specific properties such as biocompatibility, chemical stability, antibacterial activity [77–81], both using the best processing technology and theoretical study in order to have new interesting applications and knowledge.

Supplementary Materials: The following are available online at https://www.mdpi.com/article/10.3390/coatings11040420/s1. Figure S1. Scheme of the eight different initial non-optimized geometries discussed in Section 3.1.1, considering the three α-helices of the HSA *A*-subdomain considered near the TiO_2 anatase surface, using a simulation protocol proposed in previous work [65]. Figure S2. The Albumin *A*-subdomain in the final adsorption stage on the four different TiO_2 crystallographic faces reported in Figure 5, displaying the H-bonds between the protein fragment and the solid surface. Figure S3. The Ramachandran plot of the albumin *A*-subdomain in the final adsorption stage on the four different TiO_2 crystallographic faces reported in Figure 5.

Funding: This research was funded by INSTM (Consorzio Interuniversitario Nazionale per la Scienza e Tecnologia dei Materiali) (INSTMMIP07 project) (G.R.).

Institutional Review Board Statement: Not applicable.

Informed Consent Statement: Not applicable.

Conflicts of Interest: The author declares no conflict of interest.

Abbreviations

MM	Molecular mechanics
MD	Molecular dynamics
HSA	Human serum albumin
PDB	Protein Data Bank
3D	Three-dimensional
SWCNT	Single-walled carbon nanotube
PVA	Polyvinyl alcohol
H-bond	Hydrogen bond
E_{int}	Interaction energy
E_{strain}	Strain energy
$E_{intrinsic}$	Intrinsic energy
R_g	Radius of gyration
HOPG	Highly oriented pyrolytic graphite
SASA	Solvent-accessible surface area

References

1. Silva-Bermudez, P.; Rodil, S.E. An overview of protein adsorption on metal oxide coatings for biomedical implants. *Surf. Coat. Technol.* **2013**, *233*, 147–158. [CrossRef]
2. Hoffman, A.S. Biomaterials in the nano-era. *Chin. Sci. Bull.* **2013**, *58*, 4337–4341. [CrossRef]
3. Ratner, B.D. Biomaterials: Been There, Done That, and Evolving into the Future. *Annu. Rev. Biomed. Eng.* **2019**, *21*, 171–191. [CrossRef] [PubMed]
4. Ratner, B.D.; Bryant, S.J. Biomaterials: Where We Have Been and Where We Are Going. *Annu. Rev. Biomed. Eng.* **2004**, *6*, 41–75. [CrossRef] [PubMed]
5. Wei, Q.; Becherer, T.; Angioletti-Uberti, S.; Dzubiella, J.; Wischke, C.; Neffe, A.T.; Lendlein, A.; Ballauff, M.; Haag, R. Protein Interactions with Polymer Coatings and Biomaterials. *Angew. Chem. Int. Ed.* **2014**, *53*, 8004–8031. [CrossRef] [PubMed]
6. Young, T.H.; Lin, D.T.; Chen, L.Y. Human monocyte adhesion and activation on crystalline polymers with different morphology and wettability in vitro. *J. Biomed. Mater. Res.* **2000**, *50*, 490–498. [CrossRef]
7. Mei, Y.; Gerecht, S.; Taylor, M.; Urquhart, A.J.; Bogatyrev, S.R.; Cho, S.-W.; Davies, M.C.; Alexander, M.R.; Langer, R.S.; Anderson, D.G. Mapping the Interactions among Biomaterials, Adsorbed Proteins, and Human Embryonic Stem Cells. *Adv. Mater.* **2009**, *21*, 2781–2786. [CrossRef]
8. González-García, C.; Cantini, M.; Ballester-Beltrán, J.; Altankov, G.; Salmerón-Sánchez, M. The strength of the protein-material interaction determines cell fate. *Acta Biomater.* **2018**, *77*, 74–84. [CrossRef]
9. Chen, H.; Yuan, L.; Song, W.; Wu, Z.; Li, D. Biocompatible polymer materials: Role of protein-surface interactions. *Prog. Polym. Sci.* **2008**, *33*, 1059–1087. [CrossRef]
10. Veiseh, O.; Kievit, F.M.; Ellenbogen, R.G.; Zhang, M. Cancer Cell Invasion: Treatment and Monitoring Opportunities in Nanomedicine. *Adv. Drug Deliv. Rev.* **2011**, *63*, 582–596. [CrossRef]
11. Bencina, M.; Iglic, A.; Mozetic, M.; Junkar, I. Crystallized TiO_2 Nanosurfaces in Biomedical Applications. *Nanomaterials* **2020**, *10*, 1121. [CrossRef]
12. Kulkarni, M.; Mazare, A.; Gongadze, E.; Perutkova, S.; Kralj-Iglic, V.; Milosev, I.; Schmuki, P.; Iglic, A.; Mozetic, M. Titanium nanostructures for biomedical applications. *Nanotechnology* **2015**, *26*, 062002. [CrossRef] [PubMed]
13. Yeo, E.L.L.; Thong, P.S.P.; Soo, K.C.; Kah, J.C.Y. Protein corona in drug delivery for multimodal cancer therapy in vivo. *Nanoscale* **2018**, *10*, 2461–2472. [CrossRef] [PubMed]
14. Shin, H.; Jo, S.; Mikos, A.G. Biomimetic materials for tissue engineering. *Biomaterials* **2003**, *24*, 209–221. [CrossRef]
15. Gomes, S.; Leonor, I.B.; Mano, J.F.; Reis, R.L.; Kaplan, D.L. Natural and genetically engineered proteins for tissue engineering. *Prog. Polym. Sci.* **2012**, *37*, 1–17. [CrossRef]
16. Kurinomaru, T.; Inagaki, A.; Hoshi, M.; Nakamura, C.; Yamazoe, H. Protein microswimmers capable of delivering cells for tissue engineering applications. *Mater. Horizons* **2020**, *7*, 877–884. [CrossRef]
17. Liu, F.; Liu, C.; Zheng, B.W.; He, J.; Liu, J.; Chen, C.; Lee, I.S.; Wang, X.H.; Liu, Y. Synergistic Effects on Incorporation of beta-Tricalcium Phosphate and Graphene Oxide Nanoparticles to Silk Fibroin/Soy Protein Isolate Scaffolds for Bone Tissue Engineering. *Polymers* **2020**, *12*, 69. [CrossRef]
18. Sugiyama, N.; Masuda, T.; Shinoda, K.; Nakamura, A.; Tomita, M.; Ishihama, Y. Phosphopeptide enrichment by aliphatic hydroxyl acid-modified metal oxide chromatography for nano-LC-MS/MS in proteomics applications. *Mol. Cell Proteom.* **2007**, *6*, 1103–1109. [CrossRef]
19. Othman, Z.; Pastor, B.C.; van Rijt, S.; Habibovic, P. Understanding interactions between biomaterials and biological systems using proteomics. *Biomaterials* **2018**, *167*, 191–204. [CrossRef]
20. Cormack, A.N.; Tilocca, A. Structure and biological activity of glasses and ceramics. *Philos. Trans. R. Soc. A Math. Phys. Eng. Sci. Philos.* **2012**, *370*, 1271–1280. [CrossRef]

21. Cho, D.H.; Xie, T.; Truong, J.; Stoner, A.C.; Hahm, J.I. Recent advances towards single biomolecule level understanding of protein adsorption phenomena unique to nanoscale polymer surfaces with chemical variations. *Nano Res.* **2020**, *13*, 1295–1317. [CrossRef]
22. Htwe, E.E.; Nakama, Y.; Yamamoto, Y.; Tanaka, H.; Imanaka, H.; Ishida, N.; Imamura, K. Adsorption characteristics of various proteins on a metal surface in the presence of an external electric potential. *Colloids Surf. B. Biointerfaces* **2018**, *166*, 262–268. [CrossRef]
23. Huang, T.T.; Gomez, R.; Geng, T.; Bashir, R.; Bhunia, A.K.; Robinson, J.P.; Ladisch, M.R. Composite surface for blocking bacterial adsorption on protein biochips. *Biotechnol. Bioeng.* **2003**, *81*, 618–624. [CrossRef] [PubMed]
24. Wang, T.; Handschuh-Wang, S.; Yang, Y.; Zhuang, H.; Schlemper, C.; Wesner, D.; Schonherr, H.; Zhang, W.J.; Jiang, X. Controlled Surface Chemistry of Diamond/beta-SiC Composite Films for Preferential Protein Adsorption. *Langmuir* **2014**, *30*, 1089–1099. [CrossRef] [PubMed]
25. Matsuno, H.; Yokoyama, A.; Watari, F.; Uo, M.; Kawasaki, T. Biocompatibility and osteogenesis of refractory metal implants, titanium, hafnium, niobium, tantalum and rhenium. *Biomaterials* **2001**, *22*, 1253–1262. [CrossRef]
26. Craciun, A.M.; Focsan, M.; Magyari, K.; Vulpoi, A.; Pap, Z. Surface Plasmon Resonance or Biocompatibility-Key Properties for Determining the Applicability of Noble Metal Nanoparticles. *Materials* **2017**, *10*, 836. [CrossRef] [PubMed]
27. McGinley, E.L.; Moran, G.P.; Fleming, G.J.P. Base-metal dental casting alloy biocompatibility assessment using a human-derived three-dimensional oral mucosal model. *Acta Biomater.* **2012**, *8*, 432–438. [CrossRef]
28. Zadorozhnyy, V.Y.; Kozak, D.S.; Shi, X.; Wada, T.; Louzguine-Luzgin, D.V.; Kato, H. Mechanical properties, electrochemical behavior and biocompatibility of the Ti-based low-alloys containing a minor fraction of noble metals. *J. Alloys Compd.* **2018**, *732*, 915–921. [CrossRef]
29. Li, Y.H.; Yang, C.; Zhao, H.D.; Qu, S.G.; Li, X.Q.; Li, Y.Y. New Developments of Ti-Based Alloys for Biomedical Applications. *Materials* **2014**, *7*, 1709–1800. [CrossRef] [PubMed]
30. Stankic, S.; Suman, S.; Haque, F.; Vidic, J. Pure and multi metal oxide nanoparticles: Synthesis, antibacterial and cytotoxic properties. *J. Nanobiotechnol.* **2016**, *14*, 1–20. [CrossRef]
31. Visai, L.; De Nardo, L.; Punta, C.; Melone, L.; Cigada, A.; Imbriani, M.; Arciola, C.R. Titanium oxide antibacterial surfaces in biomedical devices. *Int. J. Artif. Organs.* **2011**, *34*, 929–946. [CrossRef]
32. De Nardo, L.; Raffaini, G.; Ganazzoli, F.; Chiesa, R. Metal surface oxidation and surface interactions. In *Surface Modification of Biomaterials: Methods, Analysis and Applications*; Williams, R., Ed.; Woodhead Publishing: Cambridge, UK, 2010; pp. 102–142, WOS: 000291542800006.
33. De Nardo, L.; Raffaini, G.; Ebramzadeh, E.; Ganazzoli, F. Titanium oxide modeling and design for innovative biomedical surfaces: A concise review. *Int. J. Artif. Organs* **2012**, *35*, 629–641. [CrossRef] [PubMed]
34. Almaguer-Flores, A.; Silva-Bermudez, P.; Galicia, R.; Rodil, S.E. Bacterial adhesion on amorphous and crystalline metal oxide coatings. *Mater. Sci. Eng. C* **2015**, *57*, 88–99. [CrossRef]
35. Sit, I.; Xu, Z.Z.; Grassian, V.H. Plasma protein adsorption on TiO_2 nanoparticles: Impact of surface adsorption on temperature-dependent structural changes. *Polyhedron* **2019**, *171*, 147–154. [CrossRef]
36. Rudramurthy, G.R.; Swamy, M.K. Potential applications of engineered nanoparticles in medicine and biology: An update. *J. Biol. Inorg. Chem.* **2018**, *23*, 1185–1204. [CrossRef] [PubMed]
37. Thakur, S.; Hashim, N.; Neogi, S.; Ray, A.K. Size-dependent adsorption and conformational changes induced in bovine serum albumin (BSA) on exposure to titanium dioxide (TiO_2) nanoparticles. *Sep. Sci. Technol.* **2017**, *52*, 421–434. [CrossRef]
38. Giacomelli, C.E.; Avena, M.J.; DePauli, C.P. Adsorption of bovine serum albumin onto TiO_2 particles. *J. Colloid Interface Sci.* **1997**, *188*, 387–395. [CrossRef]
39. Bakri, A.S.; Sandan, M.Z.; Adriyanto, F.; Raship, N.A.; Said, N.D.M.; Abdullah, S.A.; Rahim, M.S. Effect of Annealing Temperature of Titanium Dioxide Thin Films on Structural and Electrical Properties. In *AIP Conference Proceedings*; AIP Publishing LLC: Melville, NY, USA, 2017; Volume 1788, pp. 030030-1–030030-8. [CrossRef]
40. Catauro, M.; Tranquillo, E.; Dal Poggetto, G.; Pasquali, M.; Dell'Era, A.; Ciprioti, S.V. Influence of the Heat Treatment on the Particles Size and on the Crystalline Phase of TiO_2 Synthesized by the Sol-Gel Method. *Materials* **2018**, *11*, 2364. [CrossRef]
41. Catauro, M.; Dal Poggetto, G.; Risoluti, R.; Ciprioti, S.V. Thermal, chemical and antimicrobial characterization of bioactive titania synthesized by sol-gel method. *J. Therm. Anal. Calorim.* **2020**, *142*, 1767–1774. [CrossRef]
42. Giordano, C.; Saino, E.; Rimondini, L.; Pedeferri, M.P.; Visai, L.; Cigada, A.; Chiesa, R. Electrochemically induced anatase inhibits bacterial colonization on Titanium Grade 2 and Ti6Al4V alloy for dental and orthopedic devices. *Colloids Surf. B Biointerfaces* **2011**, *88*, 648–655. [CrossRef]
43. Kulkarni, M.; Mazare, A.; Park, J.; Gongadze, E.; Killian, M.S.; Kralj, S.; von der Mark, K.; Iglic, A.; Schmuki, P. Protein interactions with layers of TiO_2 nanotube and nanopore arrays: Morphology and surface charge influence. *Acta Biomater.* **2016**, *45*, 357–366. [CrossRef]
44. Raffaini, G.; Ganazzoli, F. Surface Topography Effects in Protein Adsorption on Nanostructured Carbon Allotropes. *Langmuir* **2013**, *29*, 4883–4893. [CrossRef] [PubMed]
45. Raffaini, G.; Ganazzoli, F. Surface ordering of proteins adsorbed on graphite. *J. Phys. Chem. B* **2004**, *108*, 13850–13854. [CrossRef]
46. Raffaini, G.; Ganazzoli, F. Separation of chiral nanotubes with an opposite handedness by chiral oligopeptide adsorption: A molecular dynamics study. *J. Chromatogr. A* **2015**, *1425*, 221–230. [CrossRef]

47. Ganazzoli, F.; Raffaini, G. Classical atomistic simulations of protein adsorption on carbon nanomaterials. *Curr. Opin. Colloid Interface Sci.* **2019**, *41*, 11–26. [CrossRef]
48. Raffaini, G.; Ganazzoli, F. Protein adsorption on the hydrophilic surface of a glassy polymer: A computer simulation study. *Phys. Chem. Chem. Phys* **2006**, *8*, 2765–2772. [CrossRef]
49. Bronze-Uhle, E.S.; Dias, L.F.G.; Trino, L.D.; Matos, A.A.; de Oliveira, R.C.; Lisboa, P.N. Physicochemical characterization of albumin immobilized on different TiO_2 surfaces for use in implant materials. *Colloids Surf. A Physicochem. Eng. Asp.* **2019**, *564*, 39–50. [CrossRef]
50. Pegueroles, M.; Tonda-Turo, C.; Planell, J.A.; Gil, F.J.; Aparicio, C. Adsorption of Fibronectin, Fibrinogen, and Albumin on TiO_2: Time-Resolved Kinetics, Structural Changes, and Competition Study. *Biointerface* **2012**, *7*, 48. [CrossRef]
51. Sousa, S.R.; Moradas-Ferreira, P.; Saramago, B.; Melo, L.V.; Barbosa, M.A. Human serum albumin adsorption on TiO_2 from single protein solutions and from plasma. *Langmuir* **2004**, *20*, 9745–9754. [CrossRef]
52. Zhao, F.H.; Chen, Y.M.; Hu, Y.; Lu, X.G.; Xiong, S.B.; Wu, B.Y.; Guo, Y.Q.; Huang, P.; Yang, B.C. Conformation changes of albumin and lysozyme on electrospun TiO_2 nanofibers and its effects on MSC behaviors. *Colloids Surf. B* **2020**, *185*, 110604. [CrossRef]
53. Giacomelli, C.E.; Esplandiu, M.J.; Ortiz, P.I.; Avena, M.J.; De Pauli, C.P. Ellipsometric study of bovine serum albumin adsorbed onto Ti/TiO_2 electrodes. *J. Colloid Interface Sci.* **1999**, *218*, 404–411. [CrossRef]
54. Kathiravan, A.; Anandan, S.; Renganathan, R. Interaction of colloidal TiO_2 with human serum albumin: A fluorescence quenching study. *Colloids Surf. A Physicochem. Eng. Asp.* **2009**, *333*, 91–95. [CrossRef]
55. Wu, Y.Q.; Zhang, H.M.; Wang, Y.Q. Conformational and functional changes of bovine serum albumin induced by TiO_2 nanoparticles binding. *J. Mol. Liq.* **2017**, *343*, 358–368. [CrossRef]
56. Sun, T.; Liu, L.S.; Sun, Y.; Tan, C.L.; Yao, F.; Liang, X.H.; Wang, Y.; Yang, Y.H.; Hu, X.Y.; Fan, J. Synthesis and Characterization of TiO_2 Nanoparticles: Applications in Research on the Interaction of Colloidal TiO_2 with Human Serum Albumin by Fluorescence Spectroscopy. *Anal. Sci.* **2012**, *28*, 491–496. [CrossRef] [PubMed]
57. Vergaro, V.; Carlucci, C.; Cascione, M.; Lorusso, C.; Conciauro, F.; Scremin, B.F.; Congedo, P.M.; Cannazza, G.; Citti, C.; Ciccarella, G. Interaction between Human Serum Albumin and Different Anatase TiO_2 Nanoparticles: A Nano-bio Interface Study. *Nanomater. Nanotechnol.* **2015**, *5*, 30. [CrossRef]
58. Xu, Z.Z.; Grassian, V.H. Bovine Serum Albumin Adsorption on TiO_2 Nanoparticle Surfaces: Effects of pH and Coadsorption of Phosphate on Protein-Surface Interactions and Protein Structure. *J. Phys. Chem. C* **2017**, *121*, 21763–21771. [CrossRef]
59. Raffaini, G.; Elli, S.; Ganazzoli, F. Computer simulation of bulk mechanical properties and surface hydration of biomaterials. *J. Biomed. Mater. Res. Part A* **2006**, *77*, 618–626. [CrossRef] [PubMed]
60. Raffaini, G.; Ganazzoli, F. Surface Hydration of Polymeric (Bio)Materials: A Molecular Dynamics Simulation Study. *J. Biomed. Mater. Res. Part A* **2010**, *92*, 1382–1391. [CrossRef]
61. Ozboyaci, M.; Kokh, D.B.; Corni, S.; Wade, R.C. Modeling and simulation of protein-surface interactions: Achievements and challenges. *Q. Rev. Biophys.* **2016**, *49*, e4. [CrossRef] [PubMed]
62. Raffaini, G.; Ganazzoli, F. Protein adsorption on biomaterial and nanomaterial surfaces: A molecular modeling approach to study non-covalent interactions. *J. Appl. Biomater. Biomech.* **2010**, *8*, 135–145. [CrossRef] [PubMed]
63. Raffaini, G.; Ganazzoli, F. Understanding the performance of biomaterials through molecular modeling: Crossing the bridge between their intrinsic properties and the surface adsorption of proteins. *Macromol. Biosci.* **2007**, *7*, 552–566. [CrossRef]
64. YazdanYar, A.; Aschauer, U.; Bowen, P. Interaction of biologically relevant ions and organic molecules with titanium oxide (rutile) surfaces: A review on molecular dynamics studies. *Colloids Surf. B* **2018**, *161*, 563–577. [CrossRef]
65. Raffaini, G.; Ganazzoli, F. Simulation study of the interaction of some albumin subdomains with a flat graphite surface. *Langmuir* **2003**, *19*, 3403–3412. [CrossRef]
66. Raffaini, G.; Ganazzoli, F. Adsorption of charged albumin subdomains on a graphite surface. *J. Biomed. Mater. Res. A* **2006**, *76*, 638–645. [CrossRef]
67. Raffaini, G.; Ganazzoli, F. Molecular modelling of protein adsorption on the surface of titanium dioxide polymorphs. *Philos. Trans. R. Soc. A* **2012**, *370*, 1444–1462. [CrossRef]
68. Raffaini, G.; Melone, L.; Punta, C. Understanding the topography effects on competitive adsorption on a nanosized anatase crystal: A molecular dynamics study. *Chem. Commun.* **2013**, *49*, 7581–7583. [CrossRef] [PubMed]
69. Fiorati, A.; Gambarotti, C.; Melone, L.; Pastori, N.; Punta, C.; Raffaini, G.; Truscello, A. Advanced Synthetic Techniques. In *Green Synthetic Approaches for Biologically Relevant Heterocycles*, 2nd ed.; Brahmachari, G., Ed.; Elsevier: Amsterdam, The Netherlands, 2020; Volume 1, pp. 189–206, ISBN 9780128205860. Available online: https://www.elsevier.com/books-and-journals (accessed on 8 March 2021).
70. Mashatooki, M.H.; Ebrahimzadeh, A.R.; Sardroodi, J.J.; Abbasi, A. Investigation of TiO_2 anatase (101), (100) and (110) facets as immobilizer for a potential anticancer RNA aptamer: A classical molecular dynamics simulation. *Mol. Simul.* **2019**, *45*, 849–858. [CrossRef]
71. Yan, L.; Chen, H.Z.; Jing, C.Y. TiO_2 Facets Shaped by Concentration-Dependent Surface Diffusion of Dopamine. *J. Phys. Chem. Lett.* **2019**, *10*, 898–903. [CrossRef] [PubMed]
72. Materials Studio BIOVIA; Discovery Studio and Accelrys Inc. *InsightII 2000*; Accelrys Inc.: San Diego, CA, USA, 2000. Available online: http://www.accelrys.com (accessed on 4 April 2021).

73. Young, D. *Computational Chemistry: A Practical Guide for Applying Techniques to Real World Problems*; John Wiley & Sons, Inc.: New York, NY, USA, 2001.
74. Berman, H.M.; Westbrook, J.; Feng, Z.; Gilliland, G.; Bhat, T.N.; Weissig, H.; Shindyalov, I.N.; Bourne, P.E. The Protein Data Bank. *Nucleic Acids Res.* **2000**, *28*, 235–242. [CrossRef]
75. Raffaini, G.; Ganazzoli, F. Molecular dynamics simulation of the adsorption of a fibronectin module on a graphite surface. *Langmuir* **2004**, *20*, 3371–3378. [CrossRef]
76. Barinov, N.A.; Prokhorov, V.V.; Dubrovin, E.V.; Klinov, D.V. AFM visualization at a single-molecule level of denaturated states of proteins on graphite. *Colloids Surf. B* **2016**, *146*, 777–784. [CrossRef]
77. Catauro, M.; Barrino, F.; Dal Poggetto, G.; Milazzo, M.; Blanco, I.; Ciprioti, S.V. Structure, drug absorption, bioactive and antibacterial properties of sol-gel SiO_2/ZrO_2 materials. *Ceram. Int.* **2020**, *46*, 29459–29465. [CrossRef]
78. Catauro, M.; Pagliuca, C.; Lisi, L.; Ruoppolo, G. Synthesis of alkoxide-derived V-Nb catalysts prepared by sol-gel route. *Thermochim. Acta* **2002**, *381*, 65–72. [CrossRef]
79. Catauro, M.; Bollino, F.; Papale, F.; Ferrara, C.; Mustarelli, P. Silica-polyethylene glycol hybrids synthesized by sol-gel: Biocompatibility improvement of titanium implants by coating. *Mater. Sci. Eng. C* **2015**, *55*, 118–125. [CrossRef]
80. Catauro, M.; Verardi, D.; Melisi, D.; Belotti, F.; Mustarelli, P. Novel sol-gel organic-inorganic hybrid materials for drug delivery. *J. Appl. Biomater. Funct. Mater.* **2010**, *8*, 42–51.
81. Catauro, M.; Blanco, I.; De Santis, R.; Russo, T.; Crescente, G. Synthesis of Glass Nanocomposite Powders: Structure, Thermal, and Antibacterial Study. *Macromol. Symp.* **2021**, *395*, 2000200. [CrossRef]